Chapter 15 Analytical Trial Function Method Ⅱ—Singular Elements with Crack and Notch

Song Cen
Department of Engineering Mechanics, School of Aerospace,
Tsinghua University, Beijing, 100084, China

Zhi-Fei Long
School of Mechanics & Civil Engineering, China University of
Mining & Technology, Beijing, 100083, China

Abstract This chapter continues to discuss the analytical trial function method. Here, the analytical trial function method is applied to develop the singular hybrid elements with crack and notch for the analysis of the crack and notch problems. During the analysis, the singular hybrid element is collocated in the region around the tips of the crack and notch, while the conventional displacement-based elements are used in the periphery region. Furthermore, this chapter also gives detailed discussions on the convergence of the singular element, zero energy mode, and improvement for the iteration solution method of eigenvalues. From the contents of this chapter and the previous chapter, it can be seen that, in the analytical trial function method, analytical and discrete methods can complement each other; and as a result, some challenging problems existing in FEM can be successfully solved.

Keywords finite element, analytical trial function method, singular element, crack, notch.

15.1 Introduction

In this chapter, the analytical trial function method is further applied to construct the singular hybrid elements with crack and notch in the analysis of the crack and notch problems. During the analysis, a kind of coupling mesh is employed: the singular hybrid element is collocated in the region around the tips of the crack and notch, while the conventional displacement-based elements are used in the periphery region.

Though the contents of this chapter are consistent with the sub-region mixed element method reported in Chaps. 12 and 13, however, their emphases are

different. Chaps. 12 and 13 emphasize particularly on the joint existence of the complementary and potential energy regions and on the application of the sub-region mixed variational principle, by which the mixed equations containing both stress and displacement variables are finally established. This chapter emphasizes particularly on the joint existence of the singular hybrid element and the conventional displacement-based elements in one mesh division and on the applications of the analytical trial function method and complementary energy principle, by which the stiffness equations containing only nodal displacements are finally obtained. That is to say, both approaches belong to the sub-region mixed element method, one emphasizes particularly on the sub-region mixture of the stress-based and displacement-based elements, and leads to the mixed equations; the other emphasizes particularly on the sub-region mixture of the hybrid and displacement-based elements, and leads to the stiffness equations.

Furthermore, this chapter will give detailed discussions on the convergence of the singular element, zero energy mode, and improvement for the iteration solution method of the eigenvalues.

15.2 The Basic Analytical Solutions of the Plane Crack Problem

According to Williams's theoretical analysis of the stress field at a plane crack tip[1], the analytical solutions of stresses, which can satisfy the equilibrium equations and boundary conditions, can be derived from the bi-harmonic stress function.

15.2.1 The Basic Analytical Solutions for the Symmetric Problem of Mode Ⅰ

A structure with a crack shown in Fig. 15.1 is considered. And, the coordinate system used here is also plotted in the figure (note: it is different from that given in Fig. 12.3, so the expressions of the analytical solutions for stresses are also different from those given by Sect. 12.3). In the polar coordinate system, the

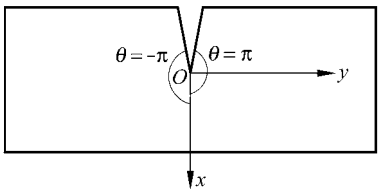

Figure 15.1 A structure with a crack

symmetric part of the bi-harmonic stress functions which satisfy equation $\nabla^4\phi=0$ can be written as

$$\phi = r^{\frac{K}{2}+1}\left[A_K\cos\left(\frac{K}{2}-1\right)\theta + B_K\cos\left(\frac{K}{2}+1\right)\theta\right] \quad (K=1,2,\cdots) \tag{15-1}$$

And, the corresponding stresses are

$$\left.\begin{aligned}
\sigma_r &= \frac{1}{r^2}\frac{\partial^2\phi}{\partial\theta^2}+\frac{1}{r}\frac{\partial\phi}{\partial r}\\
\sigma_\theta &= \frac{\partial^2\phi}{\partial r^2}\\
\tau_{r\theta} &= \frac{1}{r^2}\frac{\partial\phi}{\partial\theta}-\frac{1}{r}\frac{\partial^2\phi}{\partial\theta\partial r}=-\frac{\partial}{\partial r}\left(\frac{1}{r}\frac{\partial\phi}{\partial\theta}\right)
\end{aligned}\right\} \tag{15-2}$$

i.e.,

$$\left.\begin{aligned}
\sigma_r &= r^{\frac{K}{2}-1}\left(-\frac{K}{2}\right)\left[A_K\left(\frac{K}{2}-3\right)\cos\left(\frac{K}{2}-1\right)\theta + B_K\left(\frac{K}{2}+1\right)\right.\\
&\quad \left.\times\cos\left(\frac{K}{2}+1\right)\theta\right]\\
\sigma_\theta &= r^{\frac{K}{2}-1}\frac{K}{2}\left(\frac{K}{2}+1\right)\left[A_K\cos\left(\frac{K}{2}-1\right)\theta + B_K\cos\left(\frac{K}{2}+1\right)\theta\right]\\
\tau_{r\theta} &= r^{\frac{K}{2}-1}\frac{K}{2}\left[A_K\left(\frac{K}{2}-1\right)\sin\left(\frac{K}{2}-1\right)\theta + B_K\left(\frac{K}{2}+1\right)\sin\left(\frac{K}{2}+1\right)\theta\right]
\end{aligned}\right\} (K=1,2,\cdots) \tag{15-3}$$

For the surface of the crack with free boundary (Fig. 15.1), we have

$$\sigma_\theta\big|_{\theta=\pm\pi} = \tau_{r\theta}\big|_{\theta=\pm\pi} = 0 \tag{15-4}$$

From the last two expressions of Eq. (15-3), we can obtain

$$A_K\cos\left(\frac{K}{2}-1\right)\pi + B_K\cos\left(\frac{K}{2}+1\right)\pi = 0 \tag{15-5}$$

$$A_K\left(\frac{K}{2}-1\right)\sin\left(\frac{K}{2}-1\right)\pi + B_K\left(\frac{K}{2}+1\right)\sin\left(\frac{K}{2}+1\right)\pi = 0 \tag{15-6}$$

If A_K and B_K are both nonzero, the determinant of coefficient matrix should be zero, i.e.,

$$\begin{aligned}|\Delta| &= \left(\frac{K}{2}+1\right)\sin\left(\frac{K}{2}+1\right)\pi\cos\left(\frac{K}{2}-1\right)\pi-\left(\frac{K}{2}-1\right)\sin\left(\frac{K}{2}-1\right)\pi\cos\left(\frac{K}{2}+1\right)\pi \\ &= \left(\frac{K}{2}+1\right)[\sin K\pi+\sin 2\pi]-\left(\frac{K}{2}-1\right)[\sin K\pi-\sin 2\pi] \\ &= 2\left[\sin K\pi+\frac{K}{2}\sin 2\pi\right]=0 \end{aligned} \tag{15-7}$$

When K is an arbitrary integer, Eq. (15-7) is an identical equation. From Eqs. (15-5) and (15-6), we can obtain

$$B_K=-\frac{A_K}{K/2+1}\left[(-1)^K+\frac{K}{2}\right] \tag{15-8}$$

Let

$$A_K=\beta_{2K-1}\quad(K=1,2,\cdots) \tag{15-9}$$

then the basic analytical solutions for the stresses of the symmetric part can be written as

$$\begin{Bmatrix}\sigma_r\\ \sigma_\theta\\ \tau_{r\theta}\end{Bmatrix}=\beta_{2K-1}\begin{Bmatrix} r^{\frac{K}{2}-1}\frac{K}{2}\left[\left(3-\frac{K}{2}\right)\cos\left(\frac{K}{2}-1\right)\theta+\left(\frac{K}{2}+(-1)^K\right)\cos\left(\frac{K}{2}+1\right)\theta\right]\\ r^{\frac{K}{2}-1}\frac{K}{2}\left[\left(\frac{K}{2}+1\right)\cos\left(\frac{K}{2}-1\right)\theta-\left(\frac{K}{2}+(-1)^K\right)\cos\left(\frac{K}{2}+1\right)\theta\right]\\ r^{\frac{K}{2}-1}\frac{K}{2}\left[\left(\frac{K}{2}-1\right)\sin\left(\frac{K}{2}-1\right)\theta-\left(\frac{K}{2}+(-1)^K\right)\sin\left(\frac{K}{2}+1\right)\theta\right]\end{Bmatrix}$$
$$(K=1,2,\cdots) \tag{15-10}$$

15.2.2 The Basic Analytical Solutions for the Antisymmetric Problem of Mode Ⅱ

In the polar coordinate system, the antisymmetric part of the bi-harmonic stress functions which satisfy equation $\nabla^4\phi=0$ can be written as

$$\phi=r^{\frac{K}{2}+1}\left[C_K\sin\left(\frac{K}{2}-1\right)\theta+D_K\sin\left(\frac{K}{2}+1\right)\theta\right] \tag{15-11}$$

Similar to the symmetric problem, from the free boundary conditions of the crack surface, we can obtain

$$D_K = -\frac{C_K}{K/2+1}\left[\frac{K}{2}-(-1)^K\right] \tag{15-12}$$

Let

$$C_K = \beta_{2K} \quad (K=1,2,\cdots) \tag{15-13}$$

then the basic analytical solutions for the stresses of the antisymmetric part can be written as

$$\begin{Bmatrix}\sigma_r\\ \sigma_\theta\\ \tau_{r\theta}\end{Bmatrix} = \beta_{2K}\begin{Bmatrix} -r^{\frac{K}{2}-1}\dfrac{K}{2}\left[\left(3-\dfrac{K}{2}\right)\sin\left(\dfrac{K}{2}-1\right)\theta+\left(\dfrac{K}{2}-(-1)^K\right)\sin\left(\dfrac{K}{2}+1\right)\theta\right]\\ -r^{\frac{K}{2}-1}\dfrac{K}{2}\left[\left(\dfrac{K}{2}+1\right)\sin\left(\dfrac{K}{2}-1\right)\theta-\left(\dfrac{K}{2}-(-1)^K\right)\sin\left(\dfrac{K}{2}+1\right)\theta\right]\\ -r^{\frac{K}{2}-1}\dfrac{K}{2}\left[\left(1-\dfrac{K}{2}\right)\cos\left(\dfrac{K}{2}-1\right)\theta+\left(\dfrac{K}{2}-(-1)^K\right)\cos\left(\dfrac{K}{2}+1\right)\theta\right]\end{Bmatrix}$$
$$(K=1,2,\cdots) \tag{15-14}$$

15.2.3 The Stress Field Subspace and the Stress Intensity Factor

By selecting the first M terms of Eqs. (15-10) and (15-14), a stress field subspace with $2M$ stress parameters is then established. It can be denoted as

$$\begin{Bmatrix}\sigma_r\\ \sigma_\theta\\ \tau_{r\theta}\end{Bmatrix} = \boldsymbol{S}\begin{Bmatrix}\beta_1\\ \vdots\\ \beta_{2M}\end{Bmatrix} \tag{15-15}$$

where $\boldsymbol{S}$ is the matrix of the basic analytical solutions for stresses, which is determined by Eqs. (15-10) and (15-14).

In Eq. (15-14), when $K=2$, the stress vector is a zero vector, this term will disappear in the formulations of the stress fields.

The stress intensity factor K_{I} of mode Ⅰ is

$$K_{\mathrm{I}} = \sqrt{2\pi}\lim_{r\to 0} r^{1/2}\sigma_\theta\big|_{\theta=0} = \sqrt{2\pi}\beta_1 \tag{15-16}$$

where β_1 is the first stress parameter in Eq. (15-10).

The stress intensity factor K_{II} of mode Ⅱ is

$$K_{\mathrm{II}} = \sqrt{2\pi}\lim_{r\to 0} r^{1/2}\tau_{r\theta}\big|_{\theta=0} = -\sqrt{2\pi}\beta_2 \tag{15-17}$$

where β_2 is the first stress parameter in Eq. (15-14).

15.3 Element ATF-MS with Crack Formulated by the Analytical Trial Function Method

An element with crack is shown in Fig. 15.2. The crack surface $\theta = \pi$ and $\theta = -\pi$ are free boundaries. The outer boundary of the element contains n nodes, and there are $2n$ DOFs. The element nodal displacement vector $\boldsymbol{q}^e$ is

$$\boldsymbol{q}^e = [u_1 \quad v_1 \quad u_2 \quad v_2 \quad \cdots \quad u_n \quad v_n]^{\mathrm{T}} \tag{15-18}$$

The element stress fields are given by Eq. (15-15), in which $\boldsymbol{S}$ is a combination of the basic stress analytical solutions at the crack tip of modes Ⅰ and Ⅱ, and satisfies the equilibrium differential equations and stress boundary conditions of the crack surface. The stress parameters are

$$\boldsymbol{\beta} = [\beta_1 \quad \beta_2 \quad \cdots \quad \beta_{2M}]^{\mathrm{T}} \tag{15-19}$$

Here, the element stiffness matrix will be derived according to the minimum complementary energy principle.

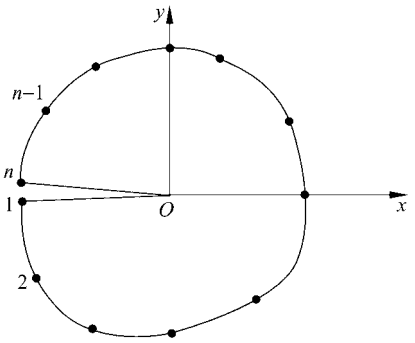

Figure 15.2 An element with crack

The complementary energy functional of the element with crack is

$$\Pi_{\mathrm{c}} = U_{\mathrm{c}} - H \tag{15-20}$$

where U_{c} is the strain complementary energy of the element; $-H$ is the complementary energy of the boundary displacements $\boldsymbol{q}^e$.

The strain complementary energy is

$$U_{\mathrm{c}} = \frac{1}{2}\iint_{\Omega} \boldsymbol{\sigma}^{\mathrm{T}} \boldsymbol{D}^{-1} \boldsymbol{\sigma} h \mathrm{d}A \tag{15-21}$$

where $\boldsymbol{D}$ is the elastic matrix

$$\boldsymbol{D}^{-1}=\frac{1}{E'}\begin{bmatrix}1 & -\mu' & 0\\ -\mu' & 1 & 0\\ 0 & 0 & 2(1+\mu')\end{bmatrix} \tag{15-22}$$

For the plane stress problem

$$E'=E,\quad \mu'=\mu \tag{15-23}$$

and for the plane strain problem

$$E'=E/(1-\mu^2),\quad \mu'=\mu/(1-\mu) \tag{15-24}$$

where E is the Young's modulus; μ is the Poisson's ratio.

Substitution of Eq. (15-15) into Eq. (15-21) yields

$$U_{\mathrm{c}}=\frac{1}{2}\boldsymbol{\beta}^{\mathrm{T}}\boldsymbol{V}\boldsymbol{\beta} \tag{15-25}$$

where

$$\boldsymbol{V}=\iint_{\Omega}\boldsymbol{S}^{\mathrm{T}}\boldsymbol{D}^{-1}\boldsymbol{S}h\mathrm{d}A \tag{15-26}$$

As to the complementary energy of the boundary displacements, we have

$$H=\int_{\Gamma}(T_x\overline{u}+T_y\overline{v})h\mathrm{d}s \tag{15-27}$$

where $\overline{u}$ and $\overline{v}$ are the element boundary displacements; T_x and T_y are the element boundary tractions

$$\begin{Bmatrix}T_x\\ T_y\end{Bmatrix}=\boldsymbol{L}\boldsymbol{S}\boldsymbol{\beta} \tag{15-28}$$

When the direction of the boundary outer normal is consistent with r-direction, the direction cosine matrix $\boldsymbol{L}$ will be

$$\boldsymbol{L}=\begin{bmatrix}\cos\theta & 0 & -\sin\theta\\ \sin\theta & 0 & \cos\theta\end{bmatrix} \tag{15-29}$$

When an angle γ exists between boundary outer normal and r, $\boldsymbol{L}$ will be

$$\boldsymbol{L}=\begin{bmatrix}\cos\theta\cos\gamma & \sin\theta\sin\gamma & -(\sin\theta\cos\gamma+\cos\theta\sin\gamma)\\ \sin\theta\cos\gamma & -\cos\theta\sin\gamma & \cos\theta\cos\gamma-\sin\theta\sin\gamma\end{bmatrix} \tag{15-30}$$

The boundary displacements can be determined by $\boldsymbol{q}^e$ and its shape function $\overline{\boldsymbol{N}}$

$$\overline{\boldsymbol{u}}=\overline{\boldsymbol{N}}\boldsymbol{q}^e \tag{15-31}$$

Equation (15-27) can be written as

$$H = \boldsymbol{\beta}^{\mathrm{T}} \boldsymbol{H} \boldsymbol{q}^{e} \tag{15-32}$$

where

$$\boldsymbol{H} = \int_{\Gamma} \boldsymbol{S}^{\mathrm{T}} \boldsymbol{L}^{\mathrm{T}} \bar{\boldsymbol{N}} h \mathrm{d}s \tag{15-33}$$

Substitution of Eqs. (15-25) and (15-32) into the expression (15-20) of the complementary energy yields

$$\Pi_{\mathrm{c}} = \frac{1}{2} \boldsymbol{\beta}^{\mathrm{T}} \boldsymbol{V} \boldsymbol{\beta} - \boldsymbol{\beta}^{\mathrm{T}} \boldsymbol{H} \boldsymbol{q}^{e} \tag{15-34}$$

From the stationary condition of the complementary energy $\delta \Pi_{\mathrm{c}} = 0$, we can obtain

$$\boldsymbol{\beta} = \boldsymbol{V}^{-1} \boldsymbol{H} \boldsymbol{q}^{e} \tag{15-35}$$

Finally, the element stiffness matrix can be derived

$$\boldsymbol{K}^{e} = \boldsymbol{H}^{\mathrm{T}} \boldsymbol{V}^{-1} \boldsymbol{H} \tag{15-36}$$

This element is denoted as ATF-MS.

15.4 Error Analysis of Element ATF-MS with Crack

A cracked plate subjected to tension load is shown in Fig. 15.3. Its stress intensity factor K_{I} has been calculated by the singular element ATF-MS, and the corresponding analysis of the convergence is also given in reference [2]. The dimensions of the plate $b = 2$ and $w = 1$; the load intensity at two sides $q = 1$; the length of the crack $a = 0.5$; the Young's modulus $E = 0.21 \times 10^{7}$; and the Poisson's ratio $\mu = 0.3$. A plane strain state is considered for this example.

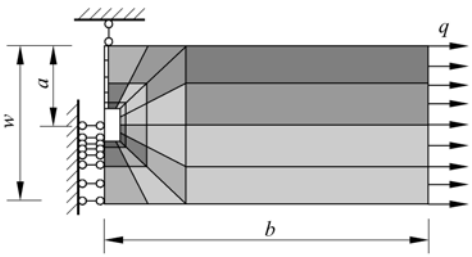

Figure 15.3 The sub-region coupled mesh of a cracked plate subjected to tension load

The mesh used is also plotted in Fig. 15.3: a singular element ATF-MS is located at the tip of the crack; around this singular element, the mesh is composed of layer-by-layer annularly distributed displacement-based elements (isoparametric element Q8), which are denser near the crack and coarser far away from the crack. In this figure, the number of the element layers along the radial direction $S_R = 3$; and the number of the element layers along the circumferential direction $4S_\theta = 8$.

The shape of the singular element ATF-MS is a square, and its half side length is R. The number of the stress terms contained in the basic analytical solutions is M (only the terms of the symmetric stress state are considered).

Here, the influences on the computational errors of the stress intensity factor K_I with variations of the following four parameters

M—the number of the stress terms used by the singular element

R—the dimension of the singular element

$4S_\theta$—the number of the element layers along the circumferential direction

S_R—the number of the element layers along the radial direction are studied.

15.4.1 Error Analysis of K_I with Variation of the Number M of Stress Terms (R = constant)

In Fig. 15.4, the longitudinal coordinate e denotes the relative error for the computational results of K_I; and the horizontal coordinate M denotes the number of the stress terms used by the singular element. Three e-M curves with $\frac{R}{a} = 0.1$, 0.3 and 0.5, respectively, are plotted. From Fig. 15.4, it can be seen that

(1) Among the three curves, errors with $\frac{R}{a} = 0.1$ are the smallest.

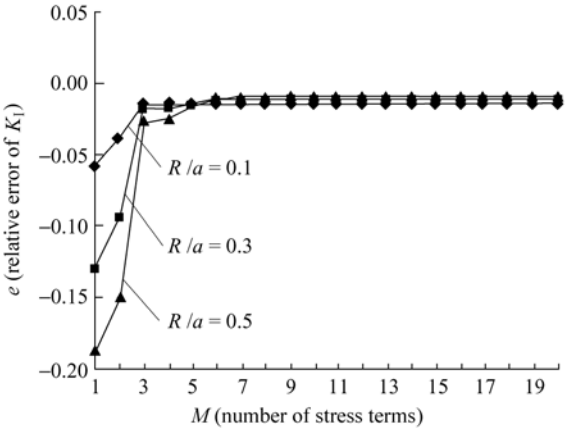

Figure 15.4 e-M curves

(2) With the increasing number M of the stress terms, the computational errors will monotonically decrease. When $M > 4$, the errors are quite small.

15.4.2 Error Analysis of K_{I} with Variation of the Dimension R of Singular Element (M = constant)

In Fig. 15.5, the longitudinal coordinate e still denotes the relative error for the computational results of K_{I}; and the horizontal coordinate $\frac{R}{a}$ denotes the ratio of the dimension R of the singular element to crack length a. Four e-$\frac{R}{a}$ curves with $M = 2$, 6, 10 and 16, respectively, are plotted. From Fig. 15.5, it can be seen that

(1) among the four curves, errors with $M = 2$ (only the first two stress terms are used) are the highest. With the increasing number M of the stress terms, errors will decrease.

(2) when $M \geqslant 6$, if the ratio $\frac{R}{a}$ varies within the range $0.03 \sim 0.3$, the computational values will tend to be stable. When $\frac{R}{a} < 0.03$, since the dimension of the singular element is too small, those adjacent displacement-based elements will be distorted, thereby, destabilization may happen in the computational results.

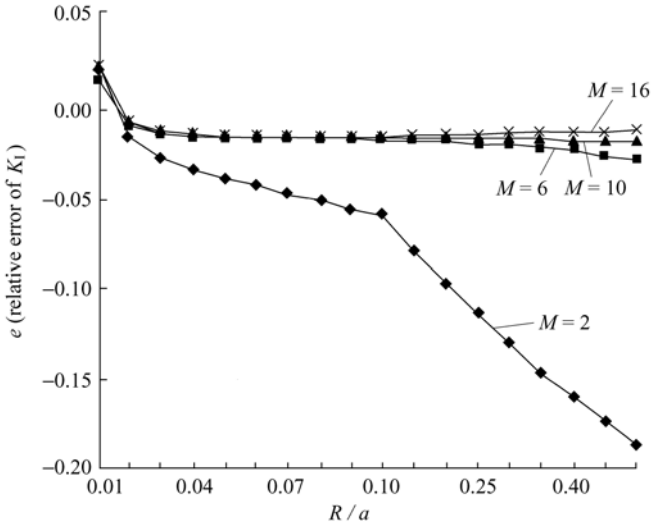

Figure 15.5 e-$\frac{R}{a}$ curves

15.4.3 Error Analysis of K_{I} with Variation of the Number S_R of Element Layers along the Radial Direction ($4S_\theta = 4$)

In Fig. 15.6, the longitudinal coordinate denotes the computational value of the stress intensity factor K_{I}; and the horizontal coordinate denotes the ratio $\frac{R}{a}$. Six curves with $S_R = 1,2,3,4,6$ and 10, respectively, are plotted (the number of the element layers along the circumferential direction $4S_\theta = 4$). From Fig. 15.6, it can be seen that

(1) Among the six curves, errors with $S_R = 1$ are the highest. When S_R increases to 10, the computational results will be quite close to the exact solutions.

(2) Since the stress fields near the crack tip vary severely along the radial direction, increase of the number S_R of the element layers along radial direction can effectively improve computational accuracy.

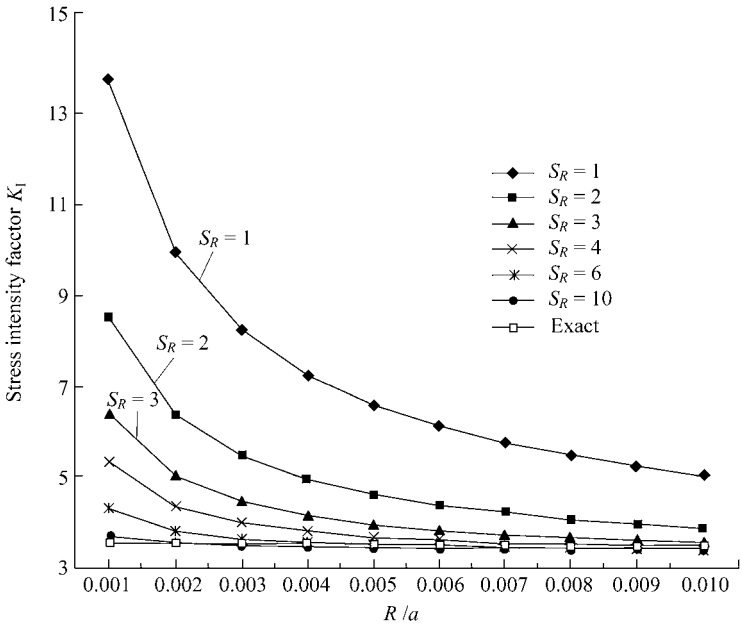

Figure 15.6 Error analysis of K_{I} with variation of the number S_R of element layers along radial direction

15.4.4 Error Analysis of K_{I} with Variation of the Number $4S_\theta$ of Element Layers along the Circumferential Direction ($S_R = 1$)

In Fig. 15.7, the longitudinal coordinate denotes the computational value of the

stress intensity factor K_{I}; and the horizontal coordinate denotes the ratio $\frac{R}{a}$. Six curves with $S_\theta = 1,2,3,4,5$ and 6, respectively, are plotted. From Fig. 15.7, it can be seen that by increasing the number $4S_\theta$ of the element layers along the circumferential direction, the precision cannot be improved significantly. This is because the circumferential variations of stress fields near the crack tip are quite gentle.

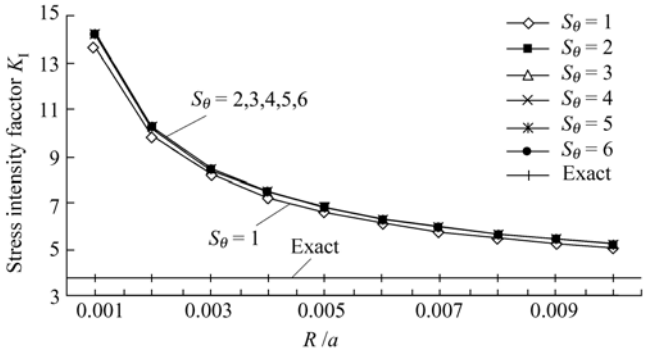

Figure 15.7 Error analysis of K_{I} with variation of the number $4S_\theta$ of element layers along circumferential direction

15.5 Analysis of Zero Energy Mode in Element and in Structural System

15.5.1 Analysis of Element Zero Energy Mode

Let us consider a plane crack problem. The coupled mesh division shown in Fig. 15.3 is employed for global analysis. Both hybrid singular element and conventional displacement-based element models simultaneously exist in the sub-region mesh, and are coupled with each other.

Assume that the stress expressions (15-15) of the hybrid stress element contains $2M$ stress parameters $\beta_i (i = 1,2,\cdots, 2M)$, and element energy is expressed by Eq. (15-34). Thereby, this element contains $2M$ independent stress (strain) modes, and the energy Π_{c} corresponding to each mode is nonzero and called as nonzero energy mode.

Assume that there are n nodes on the boundary of the hybrid singular element, so the element possesses $2n$ DOFs. Since there are $2M$ nonzero energy modes, the element has $2n - 2M$ zero energy modes. Among these $2n - 2M$ zero energy

modes, except r rigid body displacements (for plane element, $r=3$), the other zero energy modes are called as spurious zero energy modes.

Let z be the number of the element zero energy modes, and z_1 be the number of the spurious zero energy modes. Then, we have

$$\left.\begin{aligned} z &= 2n-2M \\ z_1 &= z-r = 2n-2M-r \end{aligned}\right\} \tag{15-37}$$

From the above equation, it can be seen that by properly increasing the number $2M$ of the stress terms, the number z_1 of the spurious zero energy mode can be reduced, it even becomes negative. (negative z_1 denotes that the number of the stress terms exceeds the lowest number which makes $z_1=0$)

If there are no spurious zero energy mode existing in the element, the number $2M$ of the stress terms should be not less than $2n-r$:

$$2M \geqslant 2n-r \tag{15-38}$$

In order to make further discussions on the element spurious zero energy mode, a brief introduction for the matrix eigenvalue problem is firstly given as follows.

15.5.2 Analysis of the Eigenvalues in Matrix

Let $\boldsymbol{A}$ be a n-order square matrix.

If there is a number λ satisfying

$$\boldsymbol{A}\boldsymbol{q} = \lambda \boldsymbol{q} \tag{15-39}$$

in which $\boldsymbol{q}$ is a n-order nonzero vector, then, λ is called the eigenvalue (eigenroot) of matrix $\boldsymbol{A}$; and $\boldsymbol{q}$ is the eigenvector corresponding to the eigenvalue λ. The eigenvalue λ and its corresponding eigenvector $\boldsymbol{q}$ are called characteristic pair.

The eigenmatrix of matrix $\boldsymbol{A}$ is defined by

$$\boldsymbol{A}-\lambda\boldsymbol{I} = \begin{bmatrix} a_{11}-\lambda & a_{12} & \cdots & a_{1n} \\ a_{21} & a_{22}-\lambda & \cdots & a_{2n} \\ \vdots & \vdots & \vdots & \vdots \\ a_{n1} & a_{n2} & \cdots & a_{nn}-\lambda \end{bmatrix} \tag{15-40}$$

in which $\boldsymbol{I}$ is the n-order identity matrix.

The characteristic equation of matrix $\boldsymbol{A}$ is defined by

$$\left| \boldsymbol{A}-\lambda\boldsymbol{I} \right| = 0 \tag{15-41}$$

The left side of the above equation is the determinant of the eigenmatrix, which is called as eigenpolynomial, and denoted by

$$\varphi(\lambda) = \left| \boldsymbol{A} - \lambda \boldsymbol{I} \right| \tag{15-42}$$

The n roots $\lambda_1, \lambda_2, \cdots, \lambda_n$ of the characteristic equation $\varphi(\lambda) = 0$ are the n eigenvalues of matrix $\boldsymbol{A}$.

The nonzero solution $\boldsymbol{q}$ of the homogeneous equation

$$(\boldsymbol{A} - \lambda_i \boldsymbol{I})\boldsymbol{q} = \boldsymbol{0} \tag{15-43}$$

is the eigenvector corresponding to the eigenvalue λ_i of matrix $\boldsymbol{A}$.

These eigenvalues and eigenvectors possess the following features:

(1) The eigenvalues of real symmetric matrix are all real number.

(2) The sum of n eigenvalues of n-order square matrix $\boldsymbol{A}$ equals the trace of $\boldsymbol{A}$, i.e.,

$$\lambda_1 + \lambda_2 + \cdots + \lambda_n = a_{11} + a_{22} + \cdots + a_{nn} \tag{15-44}$$

(3) The product of n eigenvalues of n-order square matrix $\boldsymbol{A}$ equals the determinant of $\boldsymbol{A}$

$$\lambda_1 \lambda_2 \cdots \lambda_n = \left| \boldsymbol{A} \right| \tag{15-45}$$

Therefore, the necessary and sufficient condition of that matrix is invertible can also be stated as: all eigenvalues of $\boldsymbol{A}$ are nonzero.

(4) If λ_i is a simple root of the characteristic equation, there will be only one linearly independent eigenvector corresponding to λ_i; If λ_i is a k multiple root of the characteristic equation, there will be k linearly independent eigenvectors corresponding to λ_i.

15.5.3 Analysis of the Eigenvalues in Element Stiffness Matrix

Let $\boldsymbol{K}^e$ be the element stiffness matrix. Since $\boldsymbol{K}^e$ is a real symmetric matrix, all eigenvalues of $\boldsymbol{K}^e$ are real numbers.

The element strain energy U^e is a quadratic expression of the element nodal displacements

$$U^e = \frac{1}{2}(\boldsymbol{q}^e)^{\mathrm{T}} \boldsymbol{K}^e \boldsymbol{q}^e \tag{15-46}$$

where the coefficient matrix $\boldsymbol{K}^e$ is just the element stiffness matrix.

If $\boldsymbol{q}^e$ is the eigenvector of $\boldsymbol{K}^e$, and corresponding to eigenvalue λ, we have

$$\boldsymbol{K}^e \boldsymbol{q}^e = \lambda \boldsymbol{q}^e \tag{15-47}$$

Substitution of the above equation into Eq. (15-46) yields

$$U^e = \frac{\lambda}{2}(\boldsymbol{q}^e)^{\mathrm{T}} \boldsymbol{q}^e \tag{15-48}$$

Since the strain energy U^e is non-negative, we can obtain

$$\lambda \geqslant 0 \tag{15-49}$$

If $\lambda > 0$, the energy U^e corresponding to the eigenvector $\boldsymbol{q}^e$ will be greater than zero, i.e., $\boldsymbol{q}^e$ belongs to the nonzero energy modes.

If $\lambda = 0$, the energy U^e corresponding to the eigenvector $\boldsymbol{q}^e$ will equal zero, i.e., $\boldsymbol{q}^e$ belongs to the zero energy modes.

If the zero eigenvalue ($\lambda = 0$) of $\boldsymbol{K}^e$ is a k multiple root, there will be k linearly independent eigenvectors corresponding to it, therefore, the element possesses k zero energy modes.

From above, it can be seen that, there is a corresponding relationship existing in the analysis of the element zero energy modes and the analysis of the eigenvalues of the element stiffness matrix $\boldsymbol{K}^e$:

(1) If the element possesses zero energy mode, the element stiffness matrix will possess zero eigenvalue, and vice versa.

(2) If the element possesses z zero energy modes, the element stiffness matrix will possess zero eigenvalue which is a z multiple root, and vice versa.

(3) Assume that the element possesses r rigid body displacement modes:

$$r = 3 \text{ (2D element)}, \quad r = 6 \text{ (3D element)}, \quad r = 3 \text{ (plate bending element)}$$

then, the element will have r or more zero energy modes; and the element stiffness matrix will possess zero eigenvalue which is a r or more multiple root.

15.5.4 Analysis of the Zero Energy Mode in Structural System

In the previous section, the analysis of the element zero energy mode has been carried out. Now, a further discussion on the zero energy mode in structural system will be given as follows.

In global finite element analysis, the global stiffness matrix $\boldsymbol{K}$ of the structural system is established by assembling the element stiffness matrix $\boldsymbol{K}^e$ and introducing the displacement boundary conditions.

In order to ensure that the structural mechanics problem can be solved, the global stiffness matrix should be an invertible one. Thereby, $\boldsymbol{K}$ should not possess zero eigenvalue, and the structural system should not have zero energy mode, i.e., on the one hand, there is no rigid body displacement mode; on the other hand, there is no spurious zero energy mode either.

As to the first point, if the structural system has enough support conditions which can prevent rigid body displacements, the rigid body displacement modes can be eliminated when the displacement boundary conditions are introduced in the global analysis.

As to the second point, the usual treatment is: it is required that all the element stiffness matrices $\boldsymbol{K}^e$ should not possess the spurious zero energy modes; and then, the global stiffness matrix $\boldsymbol{K}$ assembled by these elements will not have the spurious zero energy mode naturally. This is just for the general case. Sometimes the following case may also happen: initially, during the stage of the element analysis, though the spurious zero energy modes happen in very few elements, there are no spurious zero energy modes existing in other elements; after global assembly, these spurious zero energy mode will disappear automatically because they are prevented by constraints, i.e., the structural system after assembly will not have spurious zero energy mode. This case will be discussed as follows.

15.5.5 Theorem for the Analysis of the Spurious Zero Energy Mode in Structural System

Now, let us go back to the plane crack problem, which will be analyzed globally by using the sub-region mixed element system given by Fig. 15.3.

For example, as shown in Fig. 15.3, the mixed mesh, which is composed of hybrid singular and conventional displacement-based elements, is used, and the number $4S_\theta$ is equal to 8, so the number of the nodes in the hybrid singular element is $n = 17$. From the computational results given by Fig. 15.4 and Fig. 15.5, it can be seen that, when the number of stress terms in the hybrid element is $M = 6$, the precisions of the results have already been quite high. Here, according to Eq. (15-37), the number of the spurious zero energy modes in the hybrid element is

$$z_1 = 2n - 2M - r = 34 - 12 - 3 = 19$$

So, it can be seen that, though 19 spurious zero energy modes appear in the individual element, satisfactory results can still be obtained for the structural computations because there is no spurious zero energy mode existing in the structural system.

In the above example, two points can be explained as follows:

(1) The structural system is composed of two parts: the dominant part is the displacement-based element part containing all nodes; and the hybrid element is just an individual element containing partial nodes.

(2) If the dominant part composed of displacement-based elements is geometrically stable, and has no spurious zero energy mode, then, no matter whether the hybrid element possesses spurious zero energy modes, the original system is also geometrically stable, and has no spurious zero energy mode.

These conclusions can be written as the following forms of theorem:

(1) A sub-region mixed element system, which is composed of displacement-based and hybrid elements, is considered. For the global system, the nodal

displacement vector is $\boldsymbol{q}$, and the stiffness matrix is $\boldsymbol{K}$. For the dominant part composed of displacement-based elements, the nodal displacement vector is still $\boldsymbol{q}$, and the stiffness matrix is $\boldsymbol{K}_0$. For the hybrid element, the nodal displacement vector is $\bar{\boldsymbol{q}}$, and the stiffness matrix is $\bar{\boldsymbol{K}}$. $\bar{\boldsymbol{q}}$ is a sub-vector of $\boldsymbol{q}$

$$\boldsymbol{q} = \begin{Bmatrix} \bar{\boldsymbol{q}} \\ \boldsymbol{q}^* \end{Bmatrix}$$

According to the assembly rule of the stiffness matrix, we have

$$\boldsymbol{K} = \boldsymbol{K}_0 + \begin{bmatrix} \bar{\boldsymbol{K}} & \boldsymbol{0} \\ \boldsymbol{0} & \boldsymbol{0} \end{bmatrix} \tag{15-50}$$

(2) The singularity theorem of stiffness matrix in the sub-region mixed element system can be stated as follows:

If $\boldsymbol{K}_0$ is a nonsingular matrix, then, no matter whether $\bar{\boldsymbol{K}}$ is singular or not, $\boldsymbol{K}$ is still a nonsingular matrix.

Proof Since $\boldsymbol{K}_0$ is a nonsingular matrix, therefore, for the arbitrary nonzero $\boldsymbol{q}$, its strain energy is

$$U_0 = \frac{1}{2}\boldsymbol{q}^{\mathrm{T}}\boldsymbol{K}_0\boldsymbol{q} > 0 \tag{15-51}$$

No matter whether $\bar{\boldsymbol{K}}$ is singular or not, for the arbitrary $\bar{\boldsymbol{q}}$, its strain energy is

$$\bar{U} = \frac{1}{2}\bar{\boldsymbol{q}}^{\mathrm{T}}\bar{\boldsymbol{K}}\bar{\boldsymbol{q}} \geqslant 0 \tag{15-52}$$

Hence, for the arbitrary nonzero $\boldsymbol{q}$, the strain energy of the original system is

$$U = \frac{1}{2}\boldsymbol{q}^{\mathrm{T}}\boldsymbol{K}\boldsymbol{q} = \frac{1}{2}\boldsymbol{q}^{\mathrm{T}}\boldsymbol{K}_0\boldsymbol{q} + \frac{1}{2}\bar{\boldsymbol{q}}^{\mathrm{T}}\bar{\boldsymbol{K}}\bar{\boldsymbol{q}} > 0 \tag{15-53}$$

Therefore, $\boldsymbol{K}$ must be a nonsingular matrix. □

(3) Theorem for the analysis of the spurious zero energy mode in the sub-region mixed element system.

The above theorem can also be stated as the theorem for the analysis of the spurious zero energy mode:

If there is no spurious zero energy mode in the dominant part composed of displacement-based elements, then, no matter whether the hybrid element contains spurious zero energy mode or not, the sub-region mixed element system will not contain the spurious zero energy mode.

By the way, here the spurious zero energy mode can exist in the hybrid element, but it is inactive because of the constraints from the dominant part.

15.6 The Basic Analytical Solutions of the Plane Notch Problem

A structure with a notch is shown in Fig. 15.8. The open angle of the notch is α. By employing the stress analysis method proposed by Williams[3] for the plane notch problem, the analytical solutions for the symmetric and antisymmetric problems can be derived.

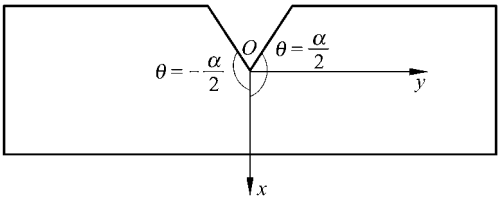

Figure 15.8 A structure with a notch

15.6.1 The Basic Analytical Solutions for Symmetric Problem of Mode Ⅰ

In polar coordinate system, the symmetric part of the bi-harmonic stress function ϕ is

$$\phi = r^{\lambda+1}[A\cos(\lambda-1)\theta + B\cos(\lambda+1)\theta] \tag{15-54}$$

Then, the corresponding stresses are

$$\left.\begin{aligned}
\sigma_r &= r^{\lambda-1}(-\lambda)[A(\lambda-3)\cos(\lambda-1)\theta + B(\lambda+1)\cos(\lambda+1)\theta] \\
\sigma_\theta &= r^{\lambda-1}\lambda(\lambda+1)[A\cos(\lambda-1)\theta + B\cos(\lambda+1)\theta] \\
\tau_{r\theta} &= r^{\lambda-1}\lambda[A(\lambda-1)\sin(\lambda-1)\theta + B(\lambda+1)\sin(\lambda+1)\theta]
\end{aligned}\right\} \tag{15-55}$$

The boundary conditions along the free edges of the notch are

$$\sigma_\theta\Big|_{\theta=\pm\frac{\alpha}{2}} = \tau_{r\theta}\Big|_{\theta=\pm\frac{\alpha}{2}} = 0$$

From the last two expressions in Eq. (15-55), we have

$$A\cos(\lambda-1)\frac{\alpha}{2} + B\cos(\lambda+1)\frac{\alpha}{2} = 0 \tag{15-56a}$$

$$A(\lambda-1)\sin(\lambda-1)\frac{\alpha}{2} + B(\lambda+1)\sin(\lambda+1)\frac{\alpha}{2} = 0 \tag{15-56b}$$

If A and B are not zero at the same time, the determinant of the coefficient matrix should be zero, i.e.,

$$\begin{aligned}|\Delta| &= (\lambda+1)\sin(\lambda+1)\frac{\alpha}{2}\cos(\lambda-1)\frac{\alpha}{2} - (\lambda-1)\sin(\lambda-1)\frac{\alpha}{2}\cos(\lambda+1)\frac{\alpha}{2} \\ &= (\lambda+1)[\sin\lambda\alpha + \sin\alpha] - (\lambda-1)[\sin\lambda\alpha - \sin\alpha] \\ &= 2[\sin\lambda\alpha + \lambda\sin\alpha] = 0 \end{aligned} \tag{15-57}$$

This is the characteristic equation of the symmetric part for the single-material V-notch problem. The eigenroots of the symmetric part can be obtained by solving Eq. (15-57). Here, these eigenroots can be both real and complex numbers. When one eigenroot is a complex number, its conjugated complex number can also satisfy the characteristic equation. So, the complex eigenroots always appear pair-wise in the form of conjugated complex numbers.

Multiply Eqs. (15-56a) and (15-56b) by $\cos\left[(\lambda+1)\frac{\alpha}{2}\right]$ and $\left(\frac{1}{\lambda+1}\right)\sin\left[(\lambda+1)\frac{\alpha}{2}\right]$ respectively, the sum of the results will be

$$A\left\{\cos\left[(\lambda-1)\frac{\alpha}{2}\right]\cos\left[(\lambda+1)\frac{\alpha}{2}\right] + \frac{\lambda-1}{\lambda+1}\sin\left[(\lambda-1)\frac{\alpha}{2}\right]\sin\left[(\lambda+1)\frac{\alpha}{2}\right]\right\} + B = 0$$

i.e.,

$$B = -A\left[\frac{\cos\lambda\alpha + \cos\alpha}{2} + \frac{\lambda-1}{\lambda+1}\left(\frac{\cos\alpha - \cos\lambda\alpha}{2}\right)\right] = -\frac{A}{\lambda+1}[\cos\lambda\alpha + \lambda\cos\alpha]$$

Let $A = 1$, then from Eq. (15-55), we obtain

$$\begin{Bmatrix}\sigma_r \\ \sigma_\theta \\ \tau_{r\theta}\end{Bmatrix} = \begin{Bmatrix} r^{\lambda-1}\lambda[(3-\lambda)\cos(\lambda-1)\theta + (\lambda\cos\alpha + \cos\lambda\alpha)\cos(\lambda+1)\theta] \\ r^{\lambda-1}\lambda[(\lambda+1)\cos(\lambda-1)\theta - (\lambda\cos\alpha + \cos\lambda\alpha)\cos(\lambda+1)\theta] \\ r^{\lambda-1}\lambda[(\lambda-1)\sin(\lambda-1)\theta - (\lambda\cos\alpha + \cos\lambda\alpha)\sin(\lambda+1)\theta] \end{Bmatrix} \tag{15-58}$$

15.6.2 The Basic Analytical Solutions for the Antisymmetric Problem of Mode Ⅱ

In the polar coordinate system, the antisymmetric part of the bi-harmonic stress function which satisfies the compatiblity equation $\nabla^4\phi = 0$ can be written as

$$\phi = r^{\lambda+1}[C\sin(\lambda-1)\theta + D\sin(\lambda+1)\theta] \tag{15-59}$$

Similar to the symmetric problem, the characteristic equation with free boundary

can be derived as

$$-\lambda\sin\alpha+\sin\lambda\alpha=0 \tag{15-60}$$

The basic analytical solutions for the antisymmetric problem of mode Ⅱ are

$$\begin{Bmatrix}\sigma_r\\ \sigma_\theta\\ \tau_{r\theta}\end{Bmatrix}=\begin{Bmatrix}-r^{\lambda-1}\lambda[(3-\lambda)\sin(\lambda-1)\theta+(\lambda\cos\alpha-\cos\lambda\alpha)\sin(\lambda+1)\theta]\\ -r^{\lambda-1}\lambda[(\lambda+1)\sin(\lambda-1)\theta-(\lambda\cos\alpha-\cos\lambda\alpha)\sin(\lambda+1)\theta]\\ -r^{\lambda-1}\lambda[(1-\lambda)\cos(\lambda-1)\theta+(\lambda\cos\alpha-\cos\lambda\alpha)\cos(\lambda+1)\theta]\end{Bmatrix} \tag{15-61}$$

15.6.3 Construction of Stress Field Subspace

Let λ_n be an arbitrary eigenroot. When λ_n is a complex root, since complex eigenroots always appear pair-wise, thereby, the real and imaginary parts of the stress solutions

$$\mathrm{Re}\begin{Bmatrix}\sigma_r\\ \sigma_\theta\\ \tau_{r\theta}\end{Bmatrix}_{\lambda=\lambda_n}\quad\text{and}\quad\mathrm{Im}\begin{Bmatrix}\sigma_r\\ \sigma_\theta\\ \tau_{r\theta}\end{Bmatrix}_{\lambda=\lambda_n} \tag{15-62}$$

can be treated as two independent stress solutions.

When λ_n is a real root, then the imaginary part will be zero, and only the real part is the nonzero stress solution.

By rationally selecting a set of basic analytical solutions corresponding to low-order eigenroots, a stress field subspace with stress parameters can be obtained and denoted by

$$\begin{Bmatrix}\sigma_r\\ \sigma_\theta\\ \tau_{r\theta}\end{Bmatrix}=\boldsymbol{S}\begin{Bmatrix}\beta_1\\ \vdots\\ \beta_{2M}\end{Bmatrix} \tag{15-63}$$

in which $\boldsymbol{S}$ is determined by Eqs. (15-58), (15-61) and (15-62).

15.6.4 Calculation of the Stress Intensity Factor

The stress intensity factor K_I of mode Ⅰ is

$$K_\mathrm{I}=\sqrt{2\pi}\lim_{r\to0}r^{1-\lambda_1}\sigma_\theta\big|_{\theta=0}=\sqrt{2\pi}\beta_1\lambda_1(\lambda_1+1-\lambda_1\cos\alpha-\cos\lambda_1\alpha) \tag{15-64}$$

where λ_1 is the minimum positive real root for the symmetric problem of mode Ⅰ; β_1 is the corresponding stress parameter.

The stress intensity factor K_{II} of mode Ⅱ is

$$\begin{aligned} K_{\mathrm{II}} &= \sqrt{2\pi}\lim_{r\to 0} r^{1-\lambda_2}\tau_{r\theta}\big|_{\theta=0} \\ &= \sqrt{2\pi}\beta_2(-\lambda_2)(1-\lambda_2+\lambda_2\cos\alpha-\cos\lambda_2\alpha) \end{aligned} \tag{15-65}$$

where λ_2 is the minimum positive real root for the antisymmetric problem of mode Ⅱ; β_2 is the corresponding stress parameter.

15.7 Element ATF-VN with Notch Formulated by the Analytical Trial Function Method

As shown in Fig. 15.9, an element with V-notch is considered. The opening angle of the notch is α. The outer circle of the element contains n nodes and $2n$ DOFs. Thus, the element nodal displacement vector is

$$\boldsymbol{q}^e = [u_1 \quad v_1 \quad u_2 \quad v_2 \quad \cdots \quad u_n \quad v_n]^{\mathrm{T}}$$

Now, the element stiffness matrix will be derived by using the analytical trial function method and the minimum complementary energy principle. This element is denoted as ATF-VN.

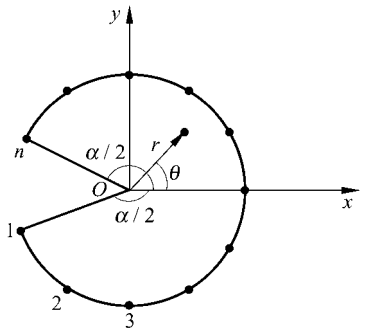

Figure 15.9 An element with V-notch

The derivation procedure is the same as that given in Sect. 15.3, and the basic formulae obtained are also the same. Now, some of them are given as follows.

The element stiffness matrix is still given by Eq. (15-36)

$$\boldsymbol{K}^e = \boldsymbol{H}^{\mathrm{T}}\boldsymbol{V}^{-1}\boldsymbol{H}$$

in which two matrices $\boldsymbol{V}$ and $\boldsymbol{H}$ on the right side are still given by Eqs. (15-26) and (15-33), respectively

$$\boldsymbol{V} = \iint_{\Omega} \boldsymbol{S}^{\mathrm{T}} \boldsymbol{D}^{-1} \boldsymbol{S} h \mathrm{d}A$$

$$\boldsymbol{H} = \int_{\Gamma} \boldsymbol{S}^{\mathrm{T}} \boldsymbol{L}^{\mathrm{T}} \bar{\boldsymbol{N}} h \mathrm{d}s$$

Except $\boldsymbol{S}$, the definitions of $\boldsymbol{D}$, $\boldsymbol{L}$, and $\bar{\boldsymbol{N}}$ are all the same as those given in Sect. 15.3.

Compared with the element with crack given in Sect. 15.3, there are two main differences existing in the element with notch given in this section:

(1) Differences of the stress fields and matrix $\boldsymbol{S}$

According to Eq. (15-15) or Eq. (15-63), the stress fields can be expressed as

$$\begin{Bmatrix} \sigma_r \\ \sigma_\theta \\ \tau_{r\theta} \end{Bmatrix} = \boldsymbol{S} \begin{Bmatrix} \beta_1 \\ \vdots \\ \beta_{2M} \end{Bmatrix}$$

But $\boldsymbol{S}$ is different from each other: in Sect. 15.3, $\boldsymbol{S}$ is determined by Eqs. (15-10) and (15-14); in this section, $\boldsymbol{S}$ is determined by Eqs. (15-58) and (15-61).

(2) Differences of the characteristic equations and eigenroots

In V-notch problem, the opening angle α of the notch is a parameter. The characteristic equations are given by Eqs. (15-57) and (15-60), and can be written as

$$\pm\lambda \sin\alpha + \sin\lambda\alpha = 0$$

The crack problem can be looked upon as a special case of the V-notch problem, in which the parameter α is assigned to be 2π.

In reference [4], there are systematical discussions on the schemes for solving eigenroots of the notch problem. In reference [5], these methods have been improved by proposing the sub-region accelerated Müller method. In Tables 15.1 and 15.2, the values of the real and imaginary parts of the first 7 eigenroot pairs $\lambda_k = \xi_k \pm \mathrm{i}\eta_k (k = 1,2,\cdots,7)$ in the notch problem are listed.

Table 15.1 The first 7 eigenroots $\lambda_k = \xi_k \pm \mathrm{i}\eta_k (k = 1,2,\cdots,7)$ of the symmetric V-notch problem of mode Ⅰ

α	ξ_1	η_1	ξ_2	η_2	ξ_3	η_3	ξ_4	η_4
190	0.900 043 76	0	1	0	2.001 795 18	0	2.695 231 53	0
200	0.818 695 81	0	1	0	2.018 264 18	0	2.420 587 07	0
210	0.751 974 51	0	1	0	2.106 286 25	0.096 100 1	3.828 293 71	0.347 176 77
220	0.697 164 94	0	1	0	2.005 648 78	0.198 379 72	3.651 102 30	0.391 981 45

(Continued)

α	ξ_1	η_1	ξ_2	η_2	ξ_3	η_3	ξ_4	η_4
230	0.652 269 53	0	1	0	1.915 272 97	0.236 951 87	3.490 348 40	0.410 599 02
240	0.615 731 04	0	1	0	1.833 548 84	0.252 251 27	3.343 717 56	0.414 037 23
250	0.586 278 85	0	1	0	1.759 251 08	0.253 998 99	3.209 376 63	0.407 444 49
260	0.562 839 47	0	1	0	1.691 413 67	0.246 340 64	3.085 831 64	0.393 570 21
270	0.544 483 72	0	1	0	1.629 257 33	0.231 250 53	2.971 843 69	0.373 931 19
280	0.530 395 71	0	1	0	1.572 143 99	0.209 446 39	2.866 373 86	0.349 278 88
290	0.519 854 30	0	1	0	1.519 546 5	0.180 478 02	2.768 545 04	0.319 765 92
300	0.512 221 36	0	1	0	1.471 027 91	0.141 852 90	2.677 615 03	0.284 901 36
310	0.506 932 84	0	1	0	1.426 227 32	0.083 159 46	2.592 958 14	0.243 187 20
320	0.503 490 48	0	1	0	1.302 693 25	0	1.467 008 48	0
330	0.501 453 01	0	1	0	1.202 957 09	0	1.490 377 81	0
340	0.500 426 37	0	1	0	1.125 406 58	0	1.497 613 49	0
350	0.500 052 99	0	1	0	1.058 842 89	0	1.499 727 77	0

α	ξ_5	η_5	ξ_6	η_6	ξ_7	η_7
190	4.022 680 43	0	4.468 956 72	0	6.142 445 45	0.110 609 04
200	4.025 002 28	0.243 014 71	5.828 632 84	0.377 126 45	7.631 219 36	0.462 931 49
210	5.547 288 43	0.459 267 73	7.264 799 21	0.536 558 54	8.981 455 32	0.596 121 47
220	5.292 797 61	0.494 878 01	6.932 731 97	0.567 288 07	8.571 681 47	0.623 509 63
230	5.061 211 04	0.507 369 59	6.630 158 89	0.576 050 10	8.198 054 26	0.629 551 95
240	4.849 458 42	0.506 015 06	6.353 222 50	0.571 559 41	7.855 910 95	0.622 700 58
250	4.655 052 57	0.495 417 26	6.098 759 71	0.558 220 72	7.541 400 85	0.607 258 88
260	4.475 934 64	0.478 103 47	5.864 131 58	0.538 470 87	7.251 297 45	0.585 613 03
270	4.310 377 17	0.455 493 56	5.647 111 62	0.513 683 79	6.982 870 25	0.559 108 24
280	4.156 917 45	0.428 313 17	5.445 805 98	0.484 565 25	6.733 791 05	0.528 434 74
290	4.014 309 24	0.396 758 19	5.258 594 12	0.451 315 66	6.502 062 99	0.493 789 48
300	3.881 487 39	0.360 496 27	5.084 084 09	0.413 644 47	6.285 966 14	0.454 895 93
310	3.757 542 54	0.318 470 43	4.921 079 46	0.370 618 18	6.084 016 40	0.410 870 72
320	2.514 054 95	0.190 785 59	3.641 705 67	0.268 252 20	4.768 557 38	0.320 170 77
330	2.440 491 94	0.114 206 83	3.533 345 48	0.203 710 63	4.625 661 14	0.257 540 31
340	2.267 186 42	0	2.476 770 05	0	3.431 990 40	0.098 448 11
350	2.118 822 72	0	2.497 979 92	0	3.181 532 51	0

Table 15.2 The first 7 eigenroots $\lambda_k = \xi_k \pm \mathrm{i}\eta_k (k = 1,2,\cdots,7)$ of the antisymmetric V-notch problem of mode Ⅱ

α	ξ_1	η_1	ξ_2	η_2	ξ_3	η_3
190	1.798 932 53	0	3.007 825 75	0	3.586 721 26	0
200	1.630 525 00	0	3.122 551 06	0.108 732 10	4.926 986 80	0.319 810 82
210	1.485 811 63	0	2.967 836 19	0.261 186 47	4.688 038 43	0.409 575 49
220	1.359 494 88	0	2.829 075 26	0.316 619 25	4.472 248 09	0.448 844 01
230	1.248 039 54	0	2.703 607 79	0.340 957 34	4.276 106 90	0.463 915 80
240	1.148 912 69	0	2.589 478 97	0.348 374 75	4.096 927 57	0.464 641 40
250	1.060 214 60	0	2.485 167 80	0.344 860 86	3.932 553 70	0.455 814 72
260	0.980 474 87	0	2.389 451 49	0.333 470 69	3.781 211 59	0.440 044 09
270	0.908 529 14	0	2.301 327 00	0.315 836 73	3.641 420 00	0.418 786 68
280	0.843 439 52	0	2.219 960 94	0.292 721 62	3.511 929 49	0.392 780 34
290	0.784 440 51	0	2.144 655 71	0.264 181 64	3.391 679 44	0.362 209 11
300	0.730 900 70	0	2.074 826 15	0.229 425 77	3.279 767 00	0.326 690 28
310	0.682 294 79	0	2.009 983 81	0.186 062 96	3.175 425 46	0.285 026 54
320	0.638 182 43	0	1.949 728 10	0.126 554 45	3.078 011 65	0.234 364 65
330	0.598 191 81	0	1.838 934 04	0	1.948 556 00	0
340	0.562 006 52	0	1.692 249 99	0	1.991 384 81	0
350	0.529 354 71	0	1.588 609 10	0	1.999 106 97	0

α	ξ_4	η_4	ξ_5	η_5	ξ_6	η_6	ξ_7	η_7
190	5.060 479 68	0	5.327 915 57	0	7.090 587 48	0.201 940 45	8.986 626 03	0.306 373 03
200	6.730 024 47	0.423 592 26	8.532 258 54	0.497 160 38	10.333 982 60	0.554 820 34	12.135 360 30	0.602 434 32
210	6.406 179 04	0.500 793 05	8.123 210 11	0.568 017 11	9.839 566 83	0.621 533 63	11.555 479 40	0.666 082 79
220	6.112 922 23	0.533 685 35	7.752 301 03	0.596 947 80	9.390 911 01	0.647 569 48	11.029 023 00	0.689 824 63
230	5.845 854 24	0.544 138 61	7.414 206 64	0.604 260 57	8.981 742 59	0.652 479 25	10.548 754 80	0.692 778 53
240	5.601 514 07	0.541 086 75	7.104 668 57	0.598 518 31	8.606 991 67	0.644 631 07	10.108 784 40	0.683 194 05
250	5.377 078 48	0.529 014 46	6.820 181 00	0.584 068 07	8.262 461 04	0.628 293 97	9.704 217 80	0.665 289 36
260	5.170 199 86	0.510 396 12	6.557 811 90	0.563 318 35	7.944 628 67	0.605 835 93	9.330 939 73	0.641 404 08
270	4.978 902 06	0.486 625 45	6.315 083 20	0.537 627 37	7.650 510 96	0.578 591 12	8.985 458 93	0.612 854 32
280	4.801 507 37	0.458 417 47	6.089 884 17	0.507 692 68	7.377 561 85	0.547 243 11	8.664 792 75	0.580 312 00
290	4.636 582 76	0.425 972 12	5.880 406 25	0.473 713 43	7.123 595 91	0.511 986 21	8.366 378 15	0.543 965 60
300	4.482 899 92	0.388 983 73	5.685 093 59	0.435 407 90	6.886 729 06	0.472 546 80	8.088 002 59	0.503 543 47
310	4.339 406 11	0.346 472 26	5.502 605 95	0.391 872 56	6.665 333 36	0.428 055 52	7.827 750 58	0.458 193 33
320	4.205 205 56	0.296 235 66	5.331 793 33	0.341 129 83	6.458 004 69	0.376 638 90	7.583 964 33	0.406 097 94
330	2.987 004 95	0.166 740 99	4.079 554 65	0.233 016 50	5.171 685 63	0.278 729 57	6.263 546 29	0.314 206 38
340	2.883 885 78	0	2.920 169 71	0	3.961 883 78	0.138 439 15	5.021 511 63	0.191 634 58
350	2.649 698 56	0	2.996 140 98	0	3.714 772 43	0	3.989 019 73	0

15.8 Error Analysis of Element ATF-VN with Notch

15.8.1 Calculation of Stress Intensity Factor K_{I} of a Specimen with V-Notch Subjected to Unidirection Tension

As an example, a specimen with V-notch subjected to unidirection tension (shown in Fig. 15.10) is considered. The error analysis of the computational results obtained by the element ATF-VN is carried out here. The dimensions of the plate are $b=1$, $w=1$ and $a=0.5$; the load density on the two sides $q=1$; the opening angle $\alpha=300^\circ$; the Young's modulus $E=0.21\times10^7$; and the Poisson's ratio $\mu=0.3$. The reference solution[6] is $K_{\mathrm{I}}=3.756$.

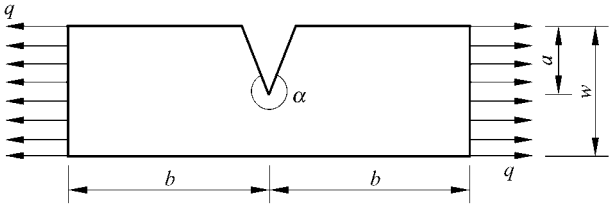

Figure 15.10 A specimen with V-notch subjected to unidirection tension

(1) The error analysis of K_{I} with variation of the number M of the stress terms (the dimension of the singular element $R=$ constant).

In Fig. 15.11, the longitudinal coordinate e denotes the relative error for the

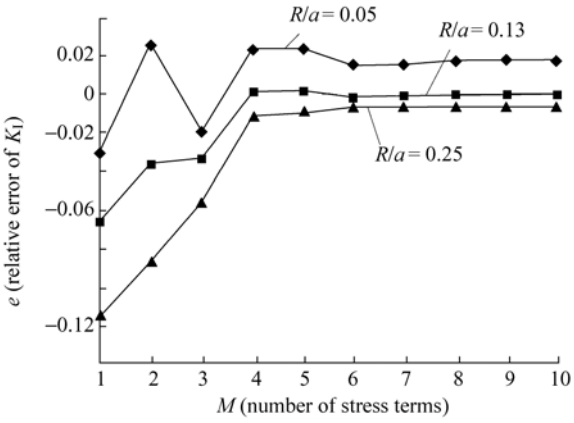

Figure 15.11 *e*-*M* curves

computational results of K_{I}; and the horizontal coordinate M denotes the number of the stress terms used by the singular element.

Three e-M curves with $\frac{R}{a}=0.05$, 0.13 and 0.25 are plotted in Fig. 15.11, respectively. These curves show that, with the increase of M, errors will decrease. When M increases to 6, the relative errors will be less than 2%.

This numerical test shows that, when $\frac{R}{a}=0.1$ and $M=6$, the effect of the global analysis is good.

(2) The error analysis of K_{I} with variation of the dimension R of the singular element ($M=$ constant)

In Fig. 15.12, the longitudinal coordinate e still denotes the relative error of K_{I}; and the horizontal coordinate $\frac{R}{a}$ denotes the ratio of the dimension R of the singular element to notch length a.

In Fig. 15.12(a), five e-$\frac{R}{a}$ curves with the number of the stress terms $M=1$, 2, 3, 4 and 5 are plotted. Among these five curves, the error is maximum when $M=1$, and minimum when $M=5$.

In Fig. 15.12(b), e-$\frac{R}{a}$ curves with the number of the stress terms $M=6$ to 10 are plotted. From these curves, it can be seen that, error e is insensitive to M; but the relation between e and $\frac{R}{a}$ is nonlinear; when $\frac{R}{a}=0.1$, the error is minimum.

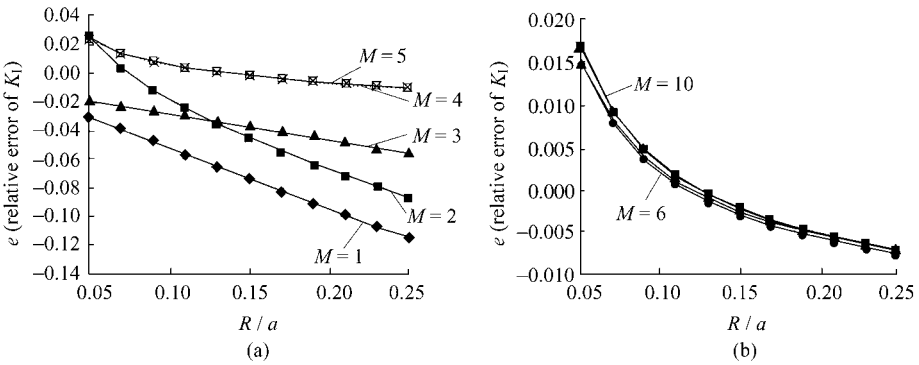

Figure 15.12 e-$\frac{R}{a}$ curves

15.8.2 Calculation of Stress Intensity Factor K_{II} of a Specimen with V-Notch Subjected to Antisymmetric Load

As an example, a specimen with V-notch shown in Fig. 15.13 is considered. The error analysis of K_{II} obtained by the element ATF-VN is carried out.

The dimensions of the specimen are $a=1$, $w=3$ and $h=1$. The Young's modulus $E=0.21\times10^7$; and the Poisson's ratio $\mu=0.3$. The resultant force $P=1$. The opening angle α of the notch varies from 360° to 330°.

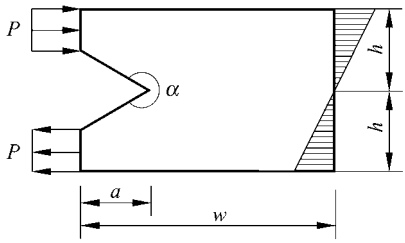

Figure 15.13 A specimen with V-notch subjected to antisymmetric load

The computational results of the stress intensity factor with different number $2M$ of the stress terms are listed in Table 15.3. From the results given by the Table, it can be seen that, when $2M=12$, the results have already been stable, and the computational errors are less than 1%.

Table 15.3 The stress intensity factor K_{II} with different number of stress terms

Number of stress terms $2M$	360°	350°	340°	330°
2	– 0.000 945 729	– 0.001 327 029	– 0.001 708 115	– 0.001 567 462
4	0.002 090 411	0.419 567 45	0.304 236 10	0.153 866 82
6	0.679 651 54	0.403 623 74	0.281 348 67	0.127 061 63
8	0.447 836 04	0.400 346 10	0.278 282 01	0.123 635 52
10	0.512 325 42	0.398 693 45	0.276 048 56	0.121 872 21
12	0.493 713 40	0.398 760 45	0.276 116 19	0.121 951 93
14	0.493 446 69	0.398 772 48	0.276 129 34	0.121 957 86
16	0.492 738 16	0.398 774 24	0.276 136 54	0.121 974 48
18	0.493 056 95	0.398 778 35	0.276 141 77	0.121 978 14
20	0.493 829 68	0.398 778 33	0.276 141 36	0.121 975 84
Reference [6]	0.500	0.401	0.278	

References

[1] Williams ML (1957) On the stress distribution at the base of a stationary crack. Journal of Applied Mechanics 24: 109 – 114

[2] Fu XR, Long YQ (2001) Fracture analysis with the sub-region mixed element method. Gong Cheng Li Xue/Engineering Mechanics 18(6): 39 – 46 (in Chinese)

[3] Williams ML (1952) Stress singularities resulting from various boundary conditions in angular corners of plates in extention. Journal of Applied Mechanics 14: 526 – 528

[4] Fan Z, Long YQ (1992) Sub-region mixed finite element analysis of V-notched plates. International Journal of Fracture 56: 333 – 344

[5] Fu XR, Long YQ (2002) Calculation of the eigenvalues—the sub-region accelerated Müller method. In: Proceedings of the Eleventh National Conference on Structural Engineering (Vol. Ⅰ). China, Changsha, pp226 – 232 (in Chinese)

[6] Gross B, Mendelson A (1972) Plane elastostatic analysis of V-notched plates. International Journal of Fracture 8: 267 – 276